Displacement response estimation of a cable-stayed bridge subjected to various loading conditions with one-dimensional residual convolutional autoencoder method

Xiaoming Lei[1,2] (iD), Dionysius M Siringoringo[3],
Zhen Sun[4] (iD) and Yozo Fujino[3]

Abstract

Displacement is an essential indicator of the functioning and safety of long-span cable-supported bridges under operational conditions. However, displacement estimation is challenging as these bridges are simultaneously subjected to various loading conditions such as temperature, wind, and vehicles. This article investigates an approach for estimating bridge displacement responses under multiple loads using a residual autoencoder model. Monitoring data of a cable-stayed bridge are collected to validate the proposed approach, including comprehensive measurements of the various loads and the displacement responses. Characteristics of temperature, wind, and vehicle loads are taken as the input, and the displacement responses at the mid-span of the main girder and top of the two pylons are taken as the output. The results showed the effectiveness of the proposed approach with an accuracy higher than 95%, which clearly outperformed other models such as long short-term memory networks in accuracy and efficiency. The effects of different types of loads are also investigated, and the wind load is found to be the most influential. Furthermore, multistep ahead prediction is carried out using the proposed approach, and good accuracy is achieved even 5 min ahead. The proposed approach can shed light on early warning of the malfunction of the bridge.

Keywords

Structural health monitoring, displacement, multistep ahead prediction, deep learning, cable-stayed bridge, surrogate model

Introduction

In recent years, numerous cable-supported bridges have been constructed worldwide to support the traffic network. They are usually built on essential routes and should be maintained in a healthy condition to ensure their serviceability and safety. After completion, bridges are subject to harsh environments such as strong winds, extreme temperature, and heavy vehicles, which poses challenges for bridge management and maintenance. The displacement responses can be used directly and indirectly for structural safety assessment as it reacts sensitively to loads applied to the structure.

Traditional routine inspection is costly in time and labor force, which is often inadequate for efficient bridge maintenance. Therefore, structural health monitoring (SHM) systems have enjoyed more popularity in long-span cable-supported bridges.[1–4] SHM can provide real-time information on bridge behavior for early warning of potential hazards and evaluation of damages in important components such as expansion joints,[5–7] stay cables,[8,9] and suspenders.[10–12] Monitored

[1]Department of Bridge Engineering, Tongji University, Shanghai, China
[2]Department of Civil and Environmental Engineering, The Hong Kong Polytechnic University, Hong Kong, China
[3]Institute of Advanced Sciences, Yokohama National University, Yokohama, Kanagawa, Japan
[4]Construct-ViBest, Faculty of Engineering (FEUP), University of Porto, Porto, Portugal

Corresponding author:
Zhen Sun, Construct-ViBest, Faculty of Engineering (FEUP), University of Porto, R. Dr. Roberto Frias, Porto, 4200-465, Portugal.
Email: sun@fe.up.pt

parameters can be categorized into input and output parameters for the bridge system.[13,14] The former includes traffic loading and environmental effects such as wind and temperature. And the latter includes bridge responses such as displacement, strain, and acceleration at concerned locations. Owing to the SHM development, the behavior of long-span bridges has been captured under thermal loads,[15,16] strong winds,[17,18] vehicles,[19,20] trainloads,[21,22] or earthquakes.[23,24]

Among the different monitored parameters, displacements of the main girder and pylon of cable-supported bridges provide important information for the functioning of bridges, and they are usually monitored with global positioning system (GPS) sensors. For example, displacement is often measured during static load test before opening for traffic, especially for long-span cable-stayed bridges.[25,26] The purpose is usually to evaluate the bridge performance according to the design requirement. Displacement responses can be obtained from acceleration measurement, but they are not very accurate. Moreover, displacement of long-span bridges is affected by various loads, such as temperature, wind, or vehicles, and they have been investigated in the past few years. Cao et al.[27] utilized the monitoring data to investigate the thermal behavior of a cable-stayed bridge with a steel box girder. The displacements of the main girder and the towers were found to be affected by the temperature variation. Based on field temperature and displacement measurements on an operational cable-stayed bridge, Zhou and Sun[28] investigated mechanisms of thermally induced variations in girder length and mid-span deflection. Liu et al.[29] proposed an approach based on long short-term memory (LSTM) network to estimate the wind spectrum, then applied a finite element (FE) bridge model to compute wind-induced buffeting responses. Westgate et al.[30] analyzed the monitored data of a suspension bridge and studied the deflection of towers and the deck during the passage of a 269-tonne trailer. These results showed an accurate match with the response predicted by an FE model of the bridge. Browhjohn et al.[31] investigated displacement responses of two suspension bridges under operational and extreme loads. A comparison of the effects of vehicular, thermal, and wind loads indicated that temperature variations dominate quasi-static response apart from rare extreme traffic and wind loads. Jesus et al.[32] developed a modular Bayesian framework to investigate the effects of temperature and traffic on displacement and natural frequency response of a suspension bridge. Results demonstrated that the bridge mid-span displacements are predicted more accurately than the natural frequencies.

Though SHM systems can directly provide the bridge responses, data interpretation is an intricate task. First, bridges are often under load effect levels much lower than the design capacity, and noise can seldom be eliminated. Second, various loads such as wind, temperature, and vehicles simultaneously affect the bridge response, which are difficult to decouple. Therefore, it is necessary to develop a robust and reliable approach to predict the displacement responses. Advances in machine learning have opened an opportunity to exploit a tremendous amount of measured data with various sources of factors involved.[33,34] Commonly used machine learning algorithms include artificial neural networks,[35–37] cluster analysis,[38] support vector machines,[39,40] and transfer learning.[41] The state-of-the-art on the application of machine learning methods in SHM of civil infrastructures was reviewed in several studies.[42–45]

An autoencoder (AE) is a type of learning architecture that employs the encoder and decoder blocks to compress the inputs to small latent features and then reconstruct the target outputs to the same size as the inputs.[46,47] Wang and Cha[48] used the AE to reconstruct the high-precision structural responses and detect structural damages. Fernandez-Navamuel et al.[49] proposed a partially explainable AE to duplicate and improve the data reduction and reconstruction ability of principal component analysis. It improves the identification capability of anomalies and allows for the detection of minor damages. Sarwar and Cantero[50] trained the AE model with the vertical acceleration data from several vehicles to detect the bridge damages. The error in signal reconstruction from the trained AE model is sensitive to damages. Li et al.[8] developed a novelty detection method based on cable force correlation using spatiotemporal graph convolutional networks, and it was verified in detecting sensor fault and structural variation of a cable-stayed bridge. Fan[51] employed AEs with skip connection to reconstruct the incomplete measured vibration data with a high loss ratio. The identified modal characteristics between the original and reconstructed signals exhibit excellent agreement. The AE model provides a stable and accurate response reconstruction method for the measured response of the structure.[52,53]

In this paper, a method is developed to predict the displacement responses of a cable-stayed bridge based on a residual autoencoder (ResAE) model, which is investigated using the monitoring data under temperature, wind, and vehicle loads simultaneously. The strengths of this model are as follows. (1) It is designed with multiple convolutional, sampling, pooling, and other layers in the architecture of encoder–decoder. The displacement response could be precisely reconstructed based on the extracted features within the different load types and between the loads and response. The residual learning is also added in each block to

alleviate the issue of gradient vanishing. (2) With the exclusion of each type of the load in the input dataset, the significance of load types could be revealed. The dominant loads might vary for each operating period. (3) The proposed model could also achieve multistep ahead response predictions. This could benefit the bridge operator in managing the structure when future responses are obtained in advance.

The remaining part of the article is organized as follows. Firstly, the cable-stayed bridge and its SHM system are introduced as a case study of the proposed method. The traffic, temperature, and wind data are presented as the input variables, while girder and pylon displacement data are described as the output variables of the prediction. Secondly, the proposed deep learning-based approach is designed to incorporate the characteristics of the multiple loads, and the model performance metrics are described. Thirdly, the model training and the predicted results are given, and the prediction accuracy represented by R^2 values are between 95.4% and 98.6% for the different outputs. Subsequently, effects of different types of loads are investigated, and the accuracy is compared with the LSTM network. A multistep ahead prediction is also explored to indicate the potential for early warning of the bridge functioning. Finally, the obtained results in this investigation are concluded, and potential merits are given for the management and maintenance of bridges.

The case-study bridge and the monitoring data

Description of the cable-stayed bridge and the SHM system

Anqing Bridge is a cable-stayed bridge on the Yangtze River that opened in 2004 in Anqing city of Anhui Province, China. It comprises a middle span of 510 m, two side spans of 215 m, and two transition spans of 50 m, respectively, as shown in Figure 1. The streamlined steel box girder has a depth of 3 m and a width of 30 m, accommodating a four-lane highway. They are supported by a fan-shaped double cable-plane system, with a total of 128 parallel-strand stay cables of the length between 92.8 m and 274.1 m. The typical distance between adjacent cables is 15 m on the deck and 2–4 m on the pylon. The bridge has two reversed-Y-shaped reinforced concrete pylons of around 184.63 m tall, which are supported by a bored pile foundation with a concrete cap. There are 12 bearings in total supporting the steel box girder vertically. At both ends of the bridge, two modular type expansion joints are installed for longitudinal movement with a capacity of 1440 mm.

To better monitor the structural behavior, an SHM system was deployed on Anqing Bridge, which includes sensors measuring wind speed and direction, temperature, strain, acceleration, displacement, and so on. This study investigates the displacement responses under multiple loads, and only the layout of the relevant sensor locations is illustrated in Figure 1. The three-dimensional supersonic anemometer is deployed in the middle of the deck on the upstream side. There are four temperature sensors installed at the cross-sections of the mid-span and the two pylons, respectively. Two GPS antennae are installed on upstream and downstream sides at the mid-span, and another two on top of the two pylons. As vehicle loads have significant influences on bridge performance, a WIM system was installed on Anqing Bridge at the entrance of the approach bridge that measured the weight and speed of the passing vehicles.

Monitoring data

The datasets extracted from SHM of the case-study bridge are introduced in this subsection. In the surrogate model, the input variables include three main types, which are traffic, wind, and temperature, respectively. The output variables include displacements of the girder and the pylon. In total, monitoring data for five successive days were collected, which started from 13:15 on December 16, 2014. Each sample was processed on a 1-min scale. As the monitoring system did not record 18 min of data, 7182 samples were finally used to establish the datasets of this study.

Traffic data. Effects of roadway traffic loads on bridge responses have been indicated as significantly influencing displacements of long-span cable-supported bridges. The traffic data are obtained from the WIM system, which covers the traffic volume, vehicle weight, and vehicles speed in each lane on the deck. In this study, six input variables are used to represent the traffic data, which are vehicle volume, vehicle average speed, and vehicle average weight on both upstream and downstream sides of the bridge. Vehicle volume is defined as the number of passing vehicles in 1 min, while vehicle average speed and vehicle average weight are obtained with all passing vehicles in 1 min.

The details of the six parameters are illustrated in Figure 2, which clearly shows the periodic characteristic of the traffic data. However, an offset of the peak positions is indicated in Figure 2(c) compared with Figure 2(a) and (b). It can be explained that the traffic volume is larger during the daytime, while it is much smaller during the night. And the vehicles during the daytime are often passenger cars which are lighter and
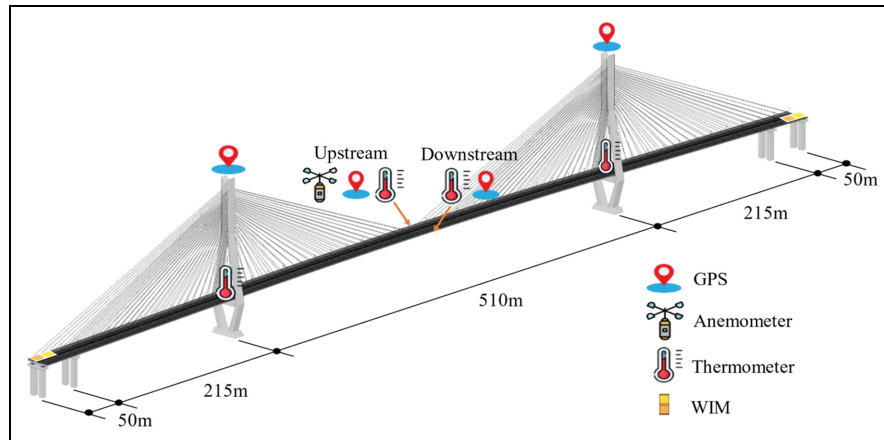
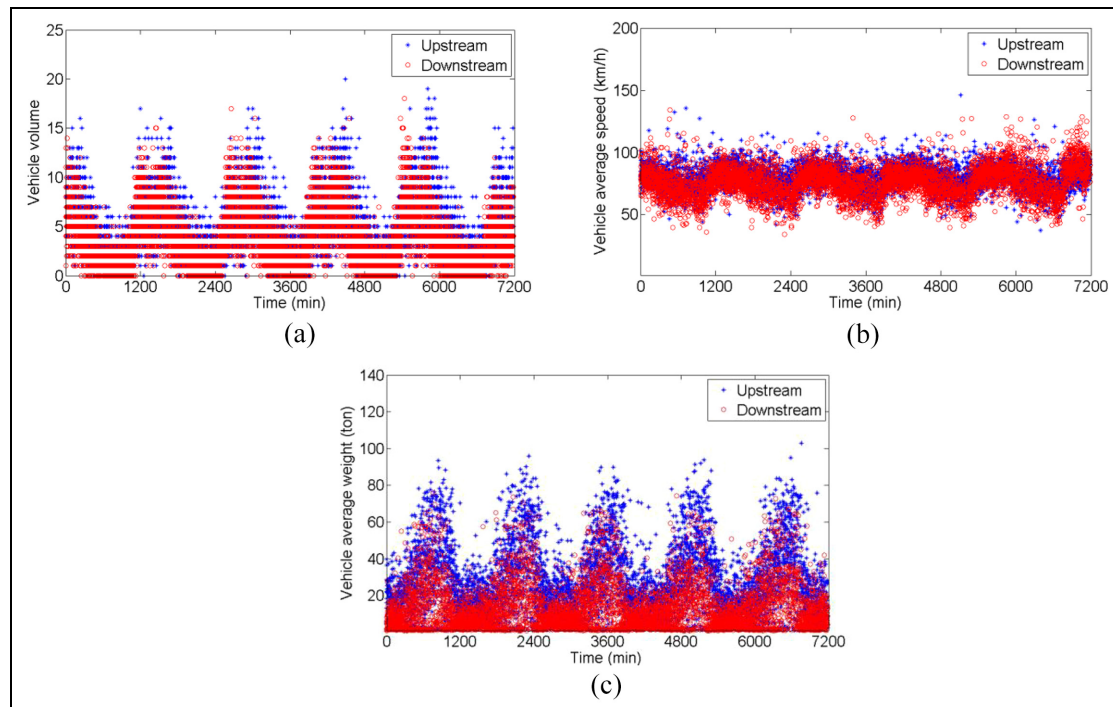**Figure 1.** Layout of the structural health monitoring system.

Figure 2. Measured traffic data. (a) Vehicle volume variation. (b) Vehicle average speed. (c) Vehicle average weight.

faster, while the freight trucks usually run at night at a lower speed. Figure 2(c) also demonstrated a larger vehicle average weight on the upstream side. The reason is that this direction leads to Anqing city, and goods are often transported to the city at night.

Temperature data. Temperature data are extracted from the four positions indicated in Figure 1, and the average is calculated as the input variable. The 1 min average temperature amplitudes in the 5 days are illustrated in Figure 3. It can be observed that there is a clearly

daily periodic pattern in the temperature data. This characteristic has been indicated by the previous studies[5,54] on monitoring data. The temperature varies between -1.3 and $13.9°C$ in this period.

Wind data. Wind data is obtained with the anemometer at the mid-span of the bridge on the upstream side. The 1-min mean values of the wind direction and wind speed are shown in Figure 4(a) and (b). The north and east are defined as $0°$ and $90°$ for the wind direction. A large variation is noticed in this period, and the
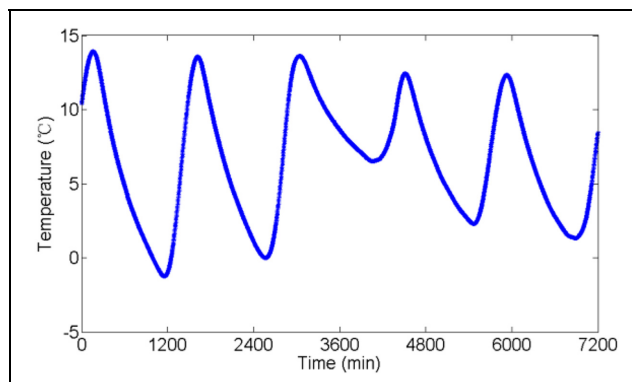
Figure 3. Temperature data.

northwest and northeast winds are dominant. The wind speed is generally under 9 m/s, indicating a relatively moderate wind.

The turbulence intensity represents the fluctuating properties of wind, which has a crucial influence on the wind-induced behavior of long-span bridges.[15] It is defined as the ratio between the standard deviation of fluctuating wind and the mean wind speed. A 1-min period is adopted to calculate the turbulence intensity, which is then processed with 10-min moving average.

$$I_i = \frac{\sigma}{U} \tag{1}$$

where σ is the standard deviation of the wind speed in the specified period; U is the mean value of the wind speed. The calculated results are shown in Figure 4(c).

Girder displacement. Girder displacements are collected on upstream and downstream sides at the mid-span in vertical, lateral, and longitudinal directions, and they are preprocessed as shown in Figure 5(a), (b), and (c), respectively. It is demonstrated that the displacements on upstream and downstream sides generally resemble each other in amplitude. The amplitude in the vertical direction is the largest, followed by the longitudinal direction, while the lateral displacement is the smallest in all three directions.

Pylon displacement. Pylon displacement data includes the longitudinal and transverse directions on top of north and south pylons, and they are shown in Figure 6(a) and (b) after preprocessing. In the longitudinal direction, the north-ward displacement is defined as positive. It is noticed that after around the second hour, the north pylon top moves south and the south pylon top move north. At around the 20th h, the moving trend is reversed. Comparing with temperature variation in Figure 3, a decrease of temperature causes the pylon tops to move toward each other and vice versa. Such a phenomenon has also been reported in another cable-
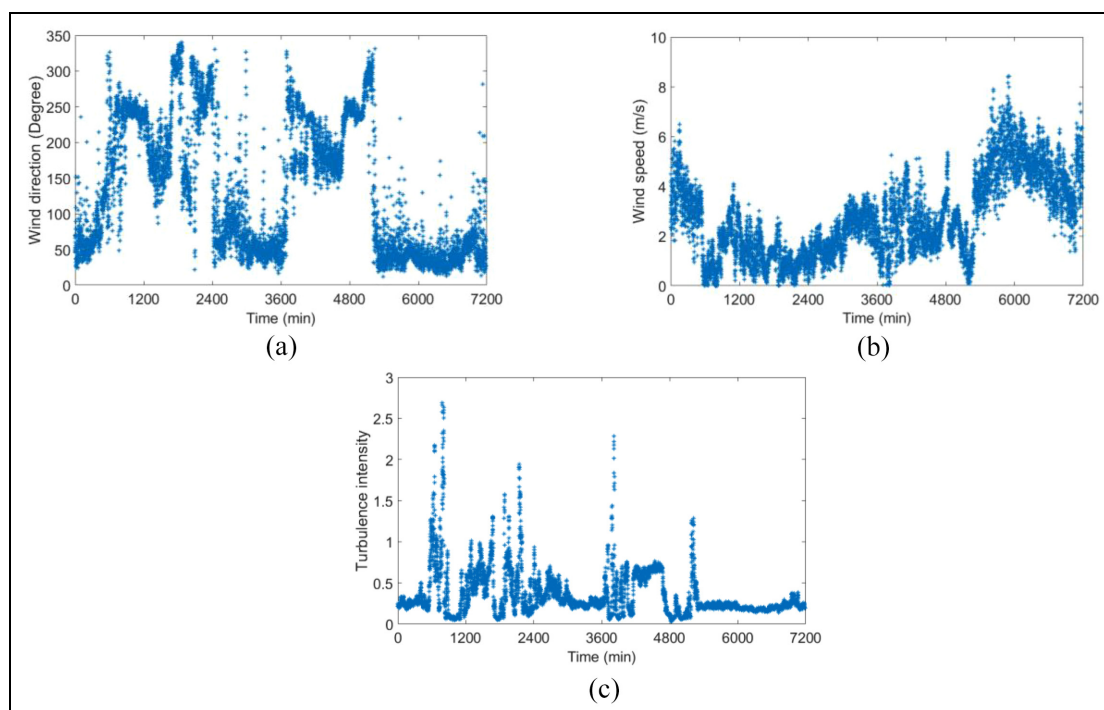

Figure 4. Measured wind data. (a) Wind direction. (b) Wind speed. (c) Turbulence intensity.
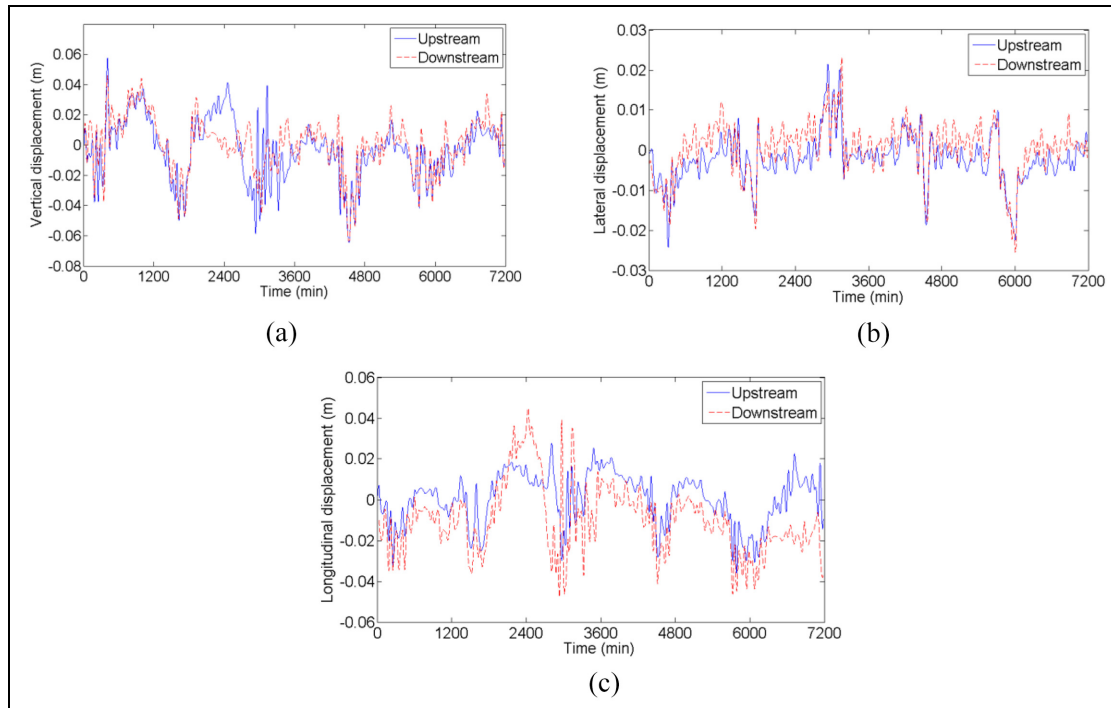
Figure 5. Measured girder mid-span displacement data. (a) Vertical displacement. (b) Lateral displacement. (c) Longitudinal displacement.
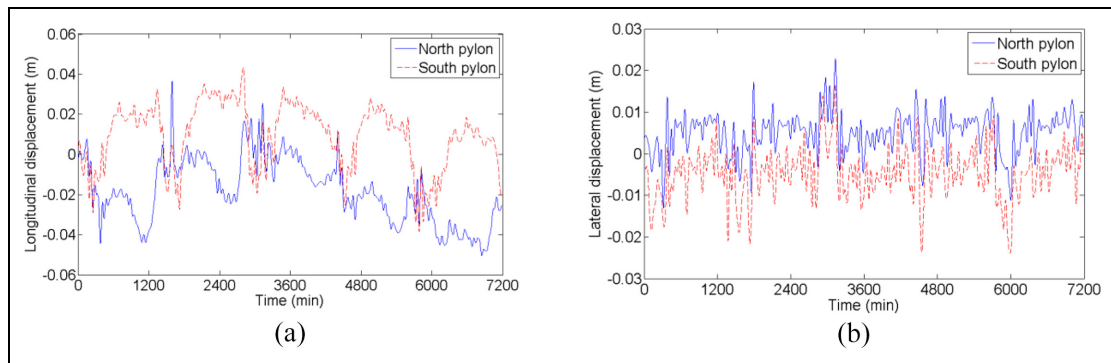

Figure 6. Measured pylon displacement data. (a) Longitudinal displacement. (b) Lateral displacement.

stayed bridge.[55] The similarity in the lateral displacement can also be observed in north and south pylons, indicating that the monitoring data have correctly captured the behavior of the pylons.

Proposed approach with one-dimensional residual convolutional AE

The proposed approach

The bridge is a complex structural system that receives the environmental and traffic loads and outputs the dynamic responses. The uncertainties and complexities within the system make it difficult to predict the responses with physics-based methods. The SHM system on the bridge records a large amount of in situ data, which contains potential correlations among loads and responses. This study uses a ResAE to construct the correlations and predict the displacement response from measured loads. An overall schematic view of the proposed approach is illustrated in Figure 7. The solid arrow lines represent the essential training steps for the ResAE model, and the dashed arrow lines represent the testing and predicting step with the untrained measured load dataset.
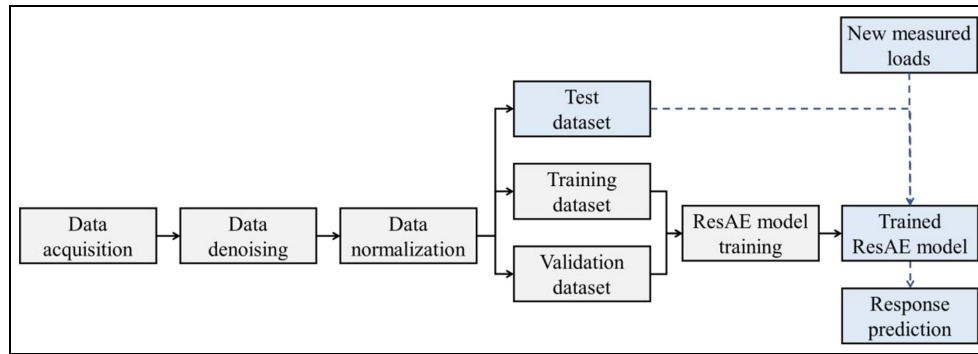
Figure 7. Framework of displacement response prediction with residual autoencoder model.

Before training the ResAE model, the acquired data should be preprocessed with the denoising and normalizing method to eliminate the effects of random noise and value range. Noises contained in the measured load data and response data are required to be removed with time-domain or frequency-domain noise reduction methods. It is difficult and unnecessary to predict the response with noise-contaminated load data or to predict the noise in the measured response. After that, the purified data is normalized with the *Z*-score strategy[56] to transfer the different ranges of fluctuation values to a similar scale. The *Z*-score normalization function is shown in Equation (2). The total dataset is randomly split into training, validation, and test dataset to train the model and determine the prediction model with the best performance. The final selected model can use load data from an untrained test dataset to predict accurate structural responses.

$$\hat{\chi} = \frac{\chi - \text{mean}\{\chi\}}{\text{standard deviation}\{\chi\}} \tag{2}$$

where $\hat{\chi}$ denotes the normalized measured data; χ denotes the original measured data; mean$\{\chi\}$ and standard deviation$\{\chi\}$ denote the mean and standard deviation values of the original measured data, respectively.

ResAE belongs to a surrogate model that can reconstruct or predict the structural responses of the measured bridge under the implemented loads. The overall ResAE method is shown in Figure 8, which sequentially contains a convolutional layer, two residual
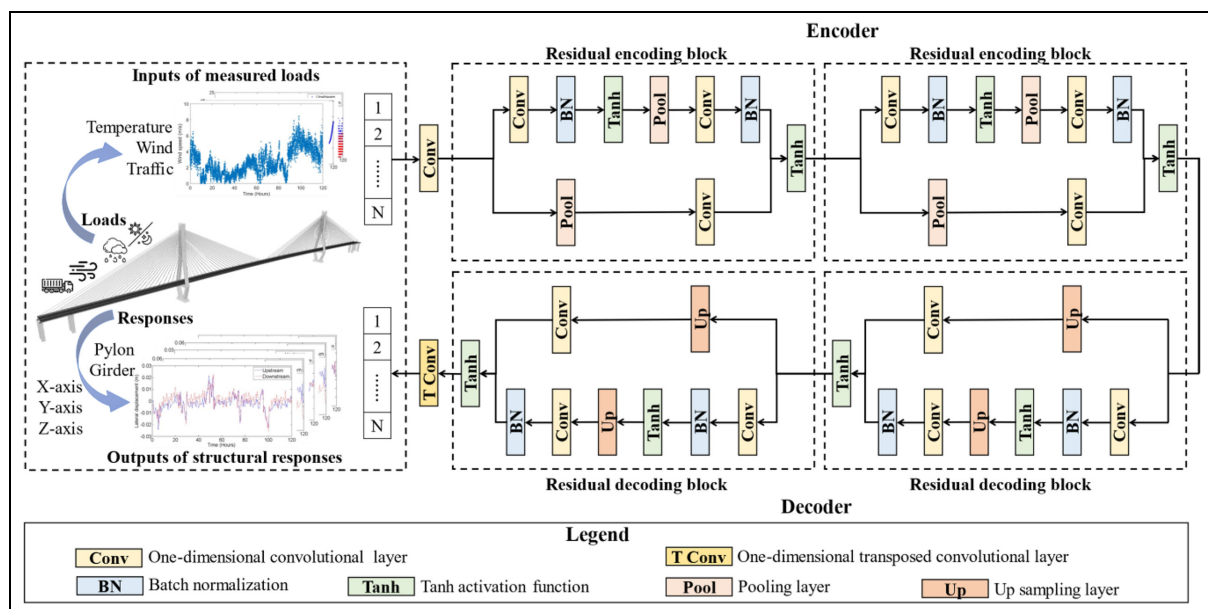

Figure 8. The one-dimensional residual convolutional autoencoder method.

encoding blocks, two residual decoding blocks, and a transposed convolutional layer. All the layers designed in this architecture are one dimensional. Critical N loads, such as temperature, wind, and traffic data, are used as inputs. The outputs are the primary N structural responses, which include three-dimensional girder and pylon displacements. The ResAE surrogate model learns from the input measured load dataset and creates reconstructed structural responses to be identical to real-world responses. The errors between reconstructed responses and ground truths are transformed into reconstruction loss to update the hyperparameters of the ResAE model. The designed multiple convolutional residual blocks allow the machine to focus on multidimensional features. It can learn the importance and correlations among extracted multilevel features, which is critical to the reconstruction problem.

AE contains an encoder–decoder structure[57] to reconstruct the data in an unsupervised manner. The encoder section is a contracting path, while the decoder section is a symmetric expanding path. The encoder receives the input measured loads and extracts latent features among the multisource data. It acts as a function f_θ, which maps an original load input subsequence x to z. While the decoder generates structure responses using the compressed features extracted by the encoder. It acts as another function g_θ, which reconstructs the output $\hat{y}$ to be measured responses y based on the extracted compressed z. The parameters embedded in the function f_θ and g_θ are free to be adjusted with the training data.

$$z = f_\theta(x) = s_f(Wx + b_w) \tag{3}$$

$$\hat{y} = g_{\theta'}(x) = s_f(Vz + b_v) \tag{4}$$

where $\theta = \{W, b_h\}$, $\theta' = \{V, b_v\}$, and s_f denotes the activation function which is the hyperbolic tangent function (Tanh) used in this architecture. W and b_h denote the weight matrix and bias vector of the encoder, while V and b_v denote the weight matrix and bias vector of the decoder.

The best behavior of AE achieves the adaptions on W, V, b_h, and b_v based on loss function in the following equation.

$$L(y - \hat{y}) = \frac{1}{N} \sum_{n=1}^{N} \left\| y^n - \hat{y}^n \right\|_2^2 \tag{5}$$

N is the total number of measured structural responses in the training dataset. Least absolute deviations (L1) and least square errors (L2) losses could measure the error between measured responses and reconstructed responses. This research employs a normalized L2 distance as the loss function since it can achieve higher training efficiency and stability.

The residual encoding and decoding blocks are important parts of the designed architecture. One of the main reasons for using residual learning is to train a very deep CNN.[58] This is because when the network aims to add many layers, the accuracy and network performance will tend to be saturated due to the problem of gradient vanishing. During the backpropagation, the gradient of the loss function concerning the weights of each layer is determined and flowed back through the neural network. Due to repeated convolution with small weights, the gradient tends to be ineffectively small in the earlier layers. Under such circumstances, the network performance inevitably degrades.

The residual connection in this architecture is not the same as the original. The original residual connection accepts an input x and produces an output $F(x) + x$, which requires $F(x)$ and x to have the same dimensions. In contrast, in the residual encoding block of the AE architecture, its output reduces the length of the data and deepens the feature depth compared to the input. Due to their inconsistent dimensions, x cannot be added directly to $F(x)$. Therefore, pooling and convolutional layers are added to the residual skip connection to solve this problem and make its output more concentrated than the input. Similarly, in the residual decoding block, an upsampling layer followed by a convolutional layer is added to the residual skip connection to match the output dimension that needs to be summed, and the output dimension can be recovered from the concentrated input.

In the residual encoding block and decoding residual block, the convolutional kernels in convolutional layers play the role of feature extractions with different scales. Thus, it can catch hidden features in different spatial dimensions. A batch normalizing layer and an activation layer follow each convolutional layer. The batch normalization is an adaptive reparameterization approach to overcome the problem of gradients vanishing and exploding caused by mini-batch training.

Model performance metrics

Statistical key performance indicators can be used to determine the model performance. The prediction errors are presented in the forms of the coefficient of determination (R^2) and root mean square error (RMSE). R^2 is a statistical measurement that analyzes the similarity between two signals, and it ranges from 0 to 1. RMSE is the standard deviation of the residuals, and it is a measure of how far the predictions is from the real data. The good model should have a high R^2 value and a low RMSE value. The R^2 and RMSE are calculated by
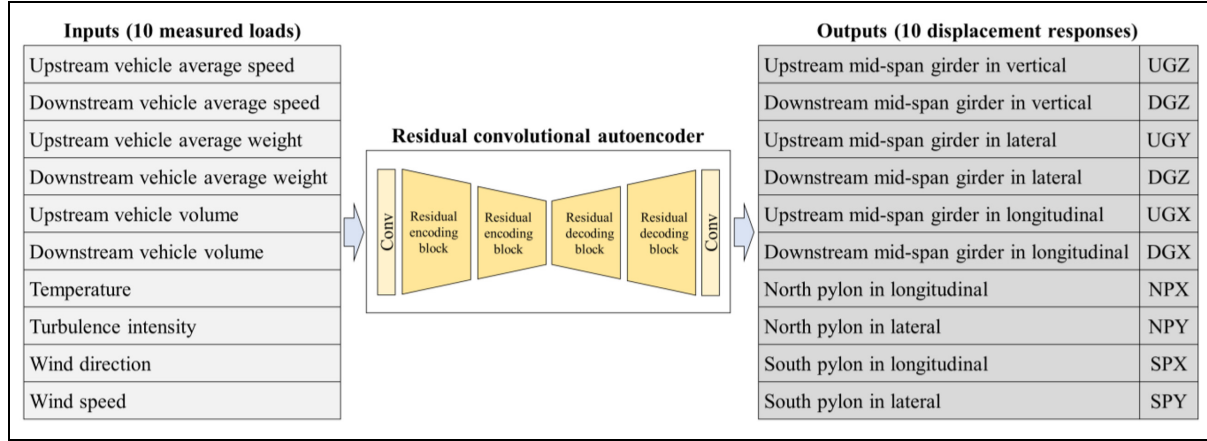
Figure 9. Application with 10 inputs and 10 outputs.

$$R^2 = 1 - \frac{\sum_{i=1}^{m} (y_i - \hat{y}_i)^2}{\sum_{i=1}^{m} (y_i - \bar{y})^2} \tag{6}$$

$$\text{RMSE} = \sqrt{\frac{1}{m} \sum_{i=1}^{m} (y_i - \hat{y}_i)^2} \tag{7}$$

where m denotes the number of data points in the dataset; y_i denotes the value in the real displacement responses; $\hat{y}_i$ denotes the value in the predicted displacement responses; and $\bar{y}$ denotes the mean value of the real displacement responses.

Prediction implementation and discussion

Model training and prediction

To implement the prediction of the displacements, it is essential to characterize the traffic, temperature, and wind loads with well-selected input variables. A total of 10 loads and 10 displacement responses were selected as the input and output variables, respectively. And they are verified to have captured the characterization of the loads. The detailed input and output variables, including the abbreviations, are shown in Figure 9.

The ResAE model is built and trained in Python 3.7 and associated libraries (Sklearn, Pytorch, etc.). It is designed to predict 10 displacement responses simultaneously. The optimal training parameters are determined with parametric studies. The one-dimensional input and output of the ResAE model are set to 10×1, and the convolution kernel size, stride size, and padding size of all the convolutional layers are set to 3, 1, and 1, respectively. The scale factor of the pooling layers and up-sampling layers is set to 2. The training epoch, batch size, and initial learning rate are 1000, 32, and 0.01, respectively. An epoch means training the

surrogate model with all the training dataset for one cycle, and an epoch is made up of one or more batches. The learning rate is changed to 1/10 of the previous value when the epoch reaches 1/2 and 3/4 of the total epoch number to keep the network stable.

As mentioned above, the dataset is randomly split into three datasets to train the ResAE model. The training, validation, and test datasets are set as 60%, 20%, and 20% of the total dataset, respectively. The ResAE model is trained with the training dataset to reduce prediction error. The validation dataset is used to determine the best weights, while the test dataset is used to determine the model efficiency. The ideal trained models should predict the structural responses accurately and have good generalization performance.

Figure 10(a) presents the training and validation loss value concerning the training epoch. It can be seen that the loss values in both the training and validation datasets are rapidly reduced at the beginning of the training and stabled at a lower value at the end of the training. Although the final validation loss is slightly higher than the training loss, the selected model also holds a good prediction performance. During the model training process, the model that produces the lowest validation loss is determined as the most optimal surrogate model. Figure 10(b) presents the coefficient of determination (R^2) between predicted and measured displacements using the most optimal ResAE model chosen in each epoch.

The predicted values and ground truth for all 10 displacement responses are compared visually in the time domain in Figure 11. Ten displacement responses are predicted using one ResAE model. Each sub-figure shows the response comparison in training, validation, and test dataset with the final ResAE model. Good agreement between real signals and predicted signals is
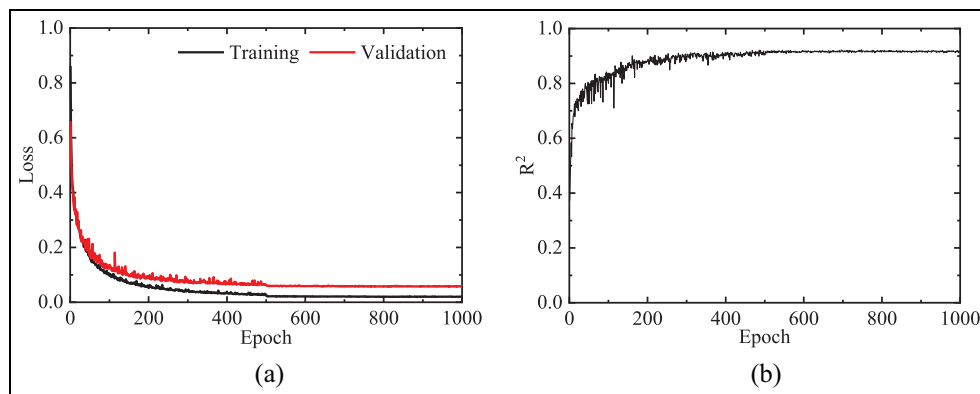
Figure 10. Loss and accuracy in each training epoch. (a) Loss. (b) Accuracy.

observed. The trend and amplitude in the time domain are well reconstructed, which indicate the effectiveness of the proposed response prediction method. Although the six displacement sensors recorded diverse structural responses at the upstream and downstream sides from three directions, the trained ResAE model captured their fluctuations well. Similar results also could be found in the responses of two pylons. The surrogate data-driven model accurately outputs bridge displacement responses after receiving the measured critical load values.

Figure 12 depicts 10 displacement response prediction performances with the aforementioned indicators. All these 10 responses have a high R^2 value and low RMSE values. The minimum and maximum R^2 values are 95.4% and 98.6%, respectively. It indicates that the predicted values are very close to the ground truth. The minimum and maximum of RMSE are 8.99×10^{-7} and 1.20×10^{-5}, respectively. The overall R^2 and RMSE of the total 10 types of displacement are 97.2% and 4.35×10^{-6}, respectively. It reveals that the response prediction performance of the proposed ResAE model is significantly guaranteed.

For the traffic and wind loads, this study investigates the impact of different types of input on the model training and prediction performance. Three representative parameters of the traffic loads are vehicle volume, vehicle average speed, and vehicle average weight. They can be calculated on upstream and downstream sides or further decomposed on each traffic lane. When using the decomposed traffic data on each lane instead of the above upstream and downstream traffic data, the overall R^2 of the trained model is 93.3%. Comparative studies were carried out showing similar performance of the model, while representation on upstream and downstream sides performs slightly better. This is due to the fact that there are only two lanes on upstream/downstream sides, and representation in the two directions (upstream and downstream)

can already capture the characteristics of traffic loads. A further decomposition into lanes causes less variation in traffic volume on each lane in the time scale. Similarly, the wind speed can be decomposed into cross-bridge and along-bridge directions as input variables. When using the decomposed wind data instead of the above original wind data, the overall R^2 of the trained model is 95.2%. The prediction results showed an equivalent level of prediction accuracy. This is mainly because the decomposed data is highly related to the original data of wind speed and direction. It is also indicated that the deep learning model could identify the correlations with good prediction accuracy. Therefore, this study recommends the use of undecomposed traffic and wind data to reduce the labor work of preprocessing in the model training.

Discussion

Effects of different types of loads. In this section, the contribution of the three different types of loads to the displacement response is investigated. During the service stage, traffic loads, temperature loads, and wind loads contribute differently to the overall response of the structure.

Each type of load will be excluded separately in the input variables to investigate their influences. Therefore, the first six traffic-related load information, the seventh temperature-related information, and the last three wind load-related information as shown in Figure 9 will be excluded in turn when training the ResAE model. They are denoted as NoTrafficLoad, NoTempLoad, NoWindLoad, respectively, in Figure 13. Suppose the accuracy of structural response prediction significantly decreases when the information of a load is excluded. In that case, it indicates that this type of load greatly influences the displacement response.

Figure 13(a) and (e) compares the ground truth and three trained models excluding each type of load in the
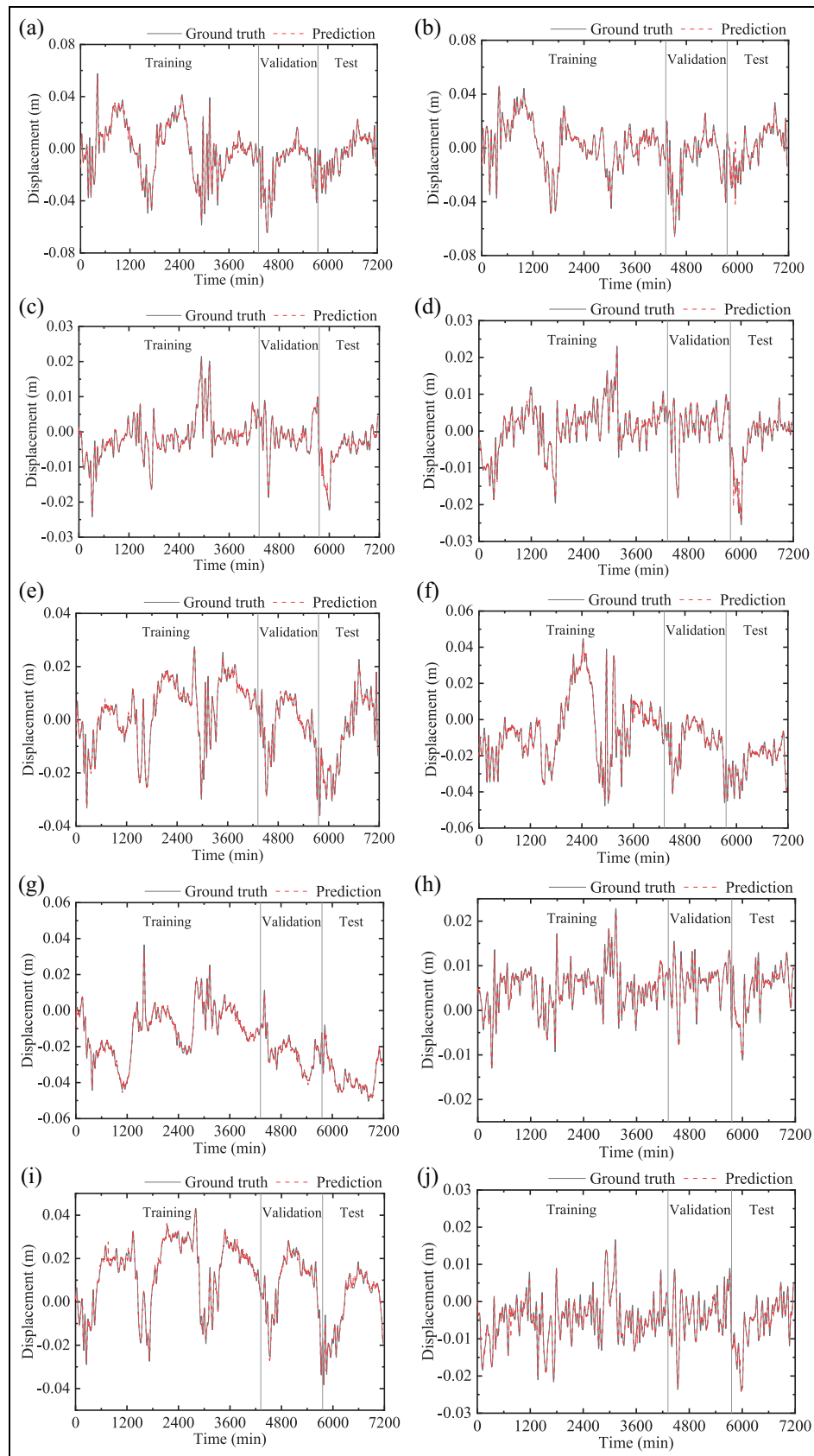
Figure 11. Comparison of predicted and measured values for each type of displacement. (a) UGZ. (b) DGZ. (c) UGY. (d) DGY. (e) UGX. (f) DGX. (g) NPX. (h) NPY. (i) SPX. (j) SPY.
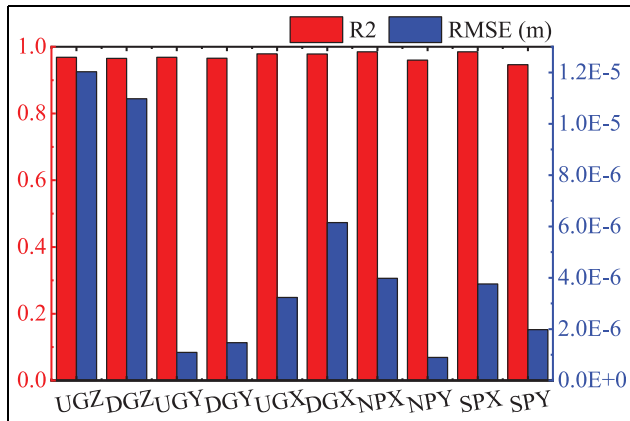
Figure 12. Performance indicators for each displacement responses.

input variables. Five representative responses are selected, including the displacements of the main girder in three directions and the displacements of the north pylon in two horizontal directions. It can be seen that when wind data are missing, the general trend of the predicted response in the vertical and lateral displacements of the main girder and the lateral displacements of the pylons are in general consistent with the contour of ground truth, but the detailed vibration information is lost. The trends and vibration details differed significantly in the bridge longitudinal displacements of both the main girder and the pylons. The effect of wind speed on the response of the cable-stayed bridge is proved to be significant. The details of the response predictions slightly deviate when traffic load or temperature load data are missing. It is the fact that the
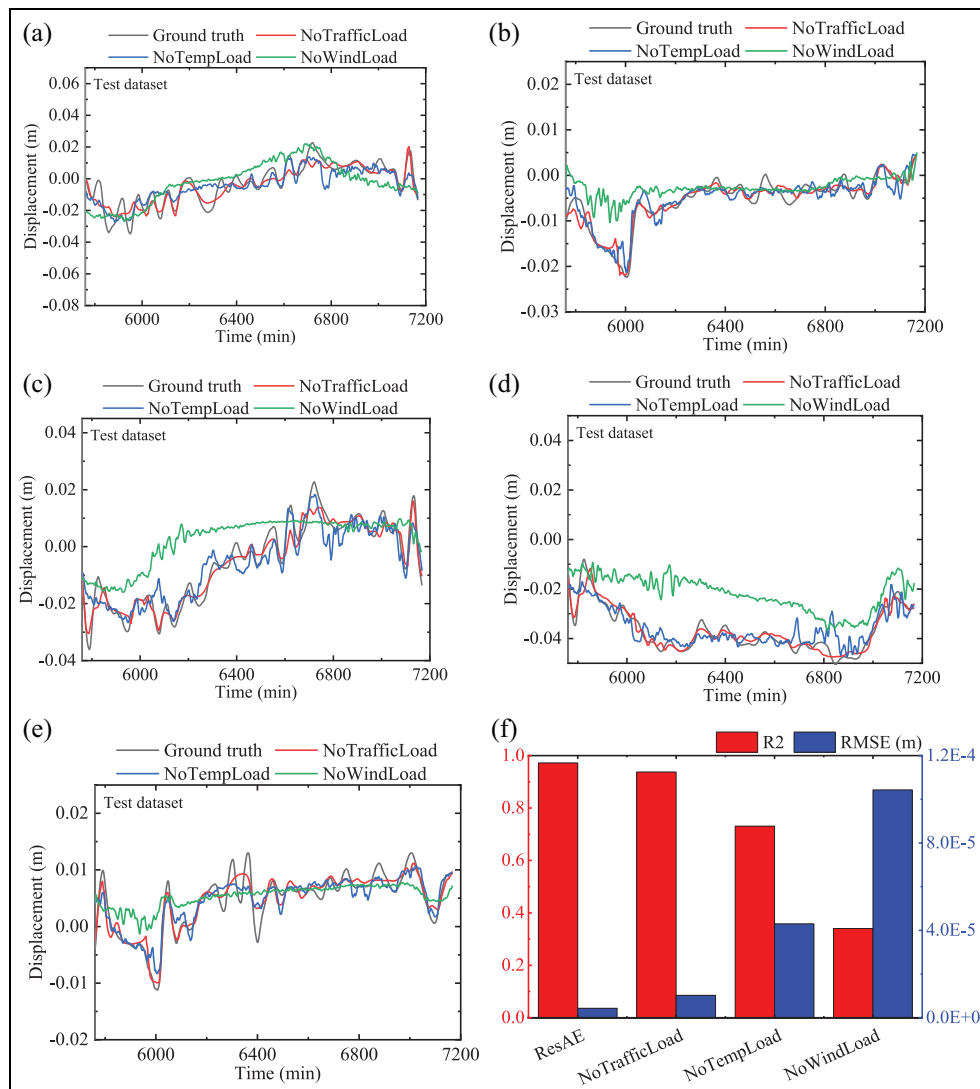

Figure 13. Effect of each type of load on predicting the structural displacement. (a) UGZ. (b) UGY. (c) UGX. (d) NPX. (e) NPY. (f) Integrated performance indicators.
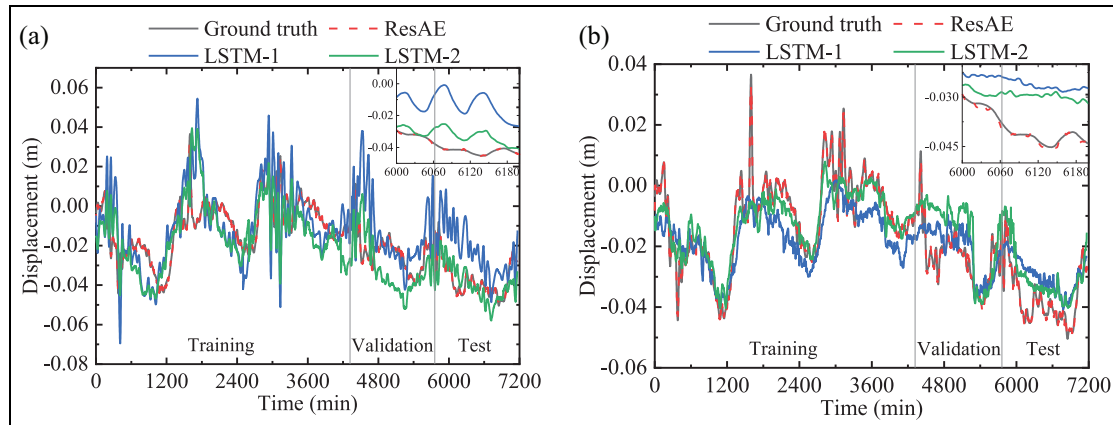
Figure 14. Comparison of different deep learning models in the test dataset. (a) UGZ. (b) NPX.

Table 1. Prediction performance of different deep learning models.

Model	R^2	RMSE	Training time (min)
ResAE	9.72×10^{-1}	4.35×10^{-6}	18.02
LSTM-1	6.90×10^{-1}	6.99×10^{-4}	152.60
LSTM-2	7.48×10^{-1}	7.76×10^{-4}	286.32

ResAE: residual autoencoder; RMSE: root mean square error; LSTM: long short-term memory.

daily traffic volume is relatively low in the cable-stayed bridge. In Figure 13(f), the integrated performance indicators, that is, R^2 and RMSE combine the corresponding indicators of each individual response. It is shown that wind has the greatest effect on the structural displacement, followed by temperature, and traffic load is the least.

Comparison with other deep learning methods. Deep learning outperforms machine learning in terms of feature extraction and output prediction. Except for the convolutional models, the recurrent models are also good at regressing and forecasting the time series data. LSTM networks are special kinds of recurrent neural networks that are capable of learning both short-term and long-term dependencies. There are three gates designed in LSTM cell to memorize the short-term and long-term features of the input time series sequence. Gates contain sigmoid activations. The first forget gate decides what information should be thrown away or kept. The second input gate decides the extent of values that should be updated. The third output gate take the output from the input gate and do a pointwise addition which updates the cell state to new values that the neural network finds relevant. For the brevity of the

article, more details on LSTM network can be found in literature.[59,60]

Thus, this section compares the prediction performance of ResAE with one-layer LSTM (LSTM-1) and two-layer LSTM (LSTM-2). The sequence length is set to 5, and the input and output sizes are set to 10 in both LSTM models. It means using 10 types of load data from the previous five moments to predict 10 structural responses under the current moment. In the LSTM block, this study designs 20 hidden neurons to memorize the time-series features. The dropout rate is set as 0.2. A dropout on the input means that for a given probability, the data on the input connection to each LSTM block will be excluded from node activation and weight updates. In addition, the LSTM-1 model and LSTM-2 model are trained with the above same dataset. Other training parameters are set as the same as the ResAE model.

Figure 14 shows the comparison of the ground truth and the predictions of three deep learning in the test dataset. The vertical displacement responses of the main girder and lateral displacement responses of the north pylon are selected as the representatives. The black solid lines (ground truth) are covered by the red dashed lines (ResAE model), and this overlapping issue can be identified from the scaled subfigures in Figure 14. This also proves that the ResAE model has a better prediction performance. By contrast, the prediction performance results of the two LSTM models differed significantly from the ground truth. The general trend of the response can be roughly presented, but the detailed features and the overall deviation are large. LSTM model exhibits high performance in establishing the input–output relationship between temperature and temperature-induced displacement[60]. But it does not work well when employing multiple loads to forecast multiple responses. Table 1 lists the performance of the three models. It can be seen that the prediction
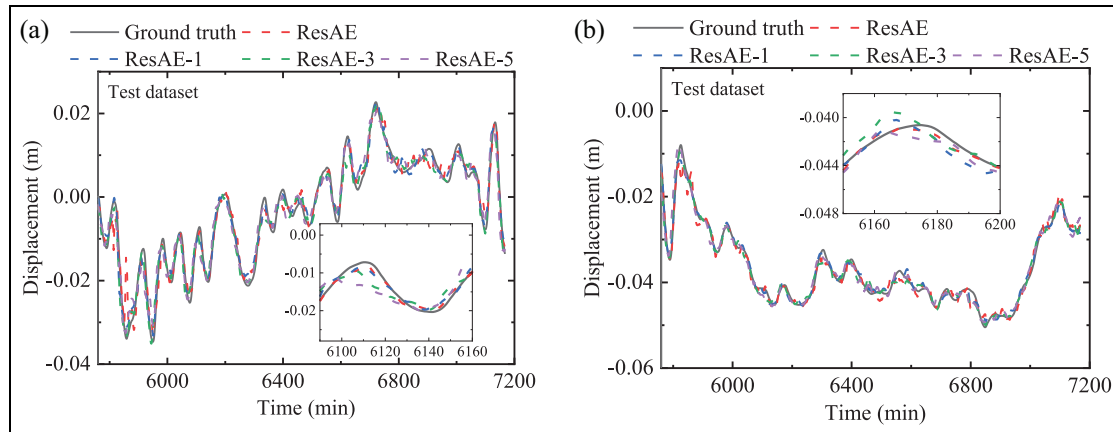
Figure 15. Comparison of predicted and measured values with different step ahead prediction models. (a) UGZ. (b) NPX.
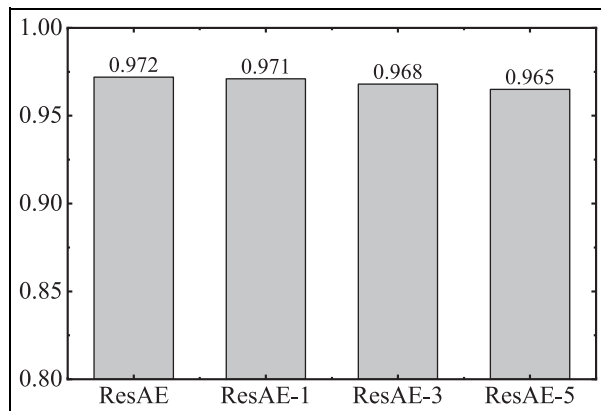

Figure 16. Coefficient of determination (R^2) for step ahead predictions.

performance of the ResAE model is better than that of the two LSTM models, and it also holds computational efficiency.

Multistep ahead prediction. In the above study, we have addressed predicting the structural displacements using load data in the same period. A more important task is to make predictions on future structural responses based on current load data. To comprehensively evaluate the predicting performance of the ResAE model, both one-step ahead and multistep ahead predictions are explored. Note that one-step ahead means 1-min ahead in this study. It is also designed to simultaneously predict the future response of 10 types of structural displacements. The training parameters of each surrogate model are the same as the above ResAE model. The prediction models with one-step ahead, three-step ahead, and five-step ahead are represented by the surrogate models ResAE-1, ResAE-3, and

ResAE-5, respectively. They are trained separately with the same dataset and training parameters as the ResAE model.

Figure 15 compares the prediction performance for the models in the test dataset at different prediction steps. The multistep ahead surrogate models provide highly comparable and reasonable patterns, whether in the main girder or pylon displacement responses. It can also be seen that there exists the lag effect in the multistep ahead prediction. As the time ahead rises, the lag effect becomes more noticeable, and the accuracy drops for both the main girders and the bridge pylons. Figure 16 shows a comparison of the R^2 metrics for different models. The R^2 are 97.2%, 97.1%, 96.8%, and 96.5% for the ResAE, ResAE-1, ResAE-3, and ResAE-5, respectively. Apparently, the one-step ahead prediction of ResAE-1 has a similar performance to the current-step prediction with ResAE. Due to the increasing absence of information, the discrepancies between the real and predicted responses gradually increase as the number of prediction intervals grows. Therefore, the proposed method can provide highly accurate step-ahead prediction for the displacement response, as evidenced by the R^2 metrics. Such step-ahead prediction ability can be used for early warning of bridge malfunction, and it will benefit the bridge operator with more reaction time to take management countermeasures.

Conclusions

This study investigates an approach for predicting bridge displacement response under temperature, wind, and vehicle loads using a one-dimensional residual convolutional AE (ResAE). Multiple convolutional residual encoding and decoding blocks are used in the ResAE to adapt to various load and response characteristics. The effectiveness and efficiency of the

proposed approach were demonstrated with a cable-stayed bridge. The relevance of load significance, model performance, and multihead prediction are discussed. The conclusions drawn from this study are summarized as follows.

(1) The proposed approach can accurately and efficiently predict a variety of displacement responses with multiple critical loads as inputs at the same time. The designed residual blocks solve the issue of gradient vanishing and assist in feature extraction and dimension matching tasks. An accuracy higher than 95% is achieved in the case study.

(2) Wind loads have the most substantial influence on structural displacement responses of cable-stayed bridges compared to traffic and temperature loads. The overall trend of the predicted response is generally compatible with the contour of ground truth when wind data is excluded, but particular vibration information is lost. When it comes to traffic or temperature loads, their exclusions only create minor differences from the expected response.

(3) The ResAE model outperformed the LSTM model in the task of the prediction of the displacement response in terms of both computational accuracy and efficiency. The general trend of the predicted response of the LSTM model can be roughly presented, but the details are missing, and the overall deviation is large.

(4) The proposed approach can complete highly accurate multistep ahead prediction on the displacement responses. As the prediction step increases, the difference between the real and predicted responses gradually increases. The prediction of structural displacement could benefit the bridge operator for online early warning of potential malfunction.

ORCID iDs

Xiaoming Lei 🆔 https://orcid.org/0000-0003-0963-3237
Zhen Sun 🆔 https://orcid.org/0000-0002-2053-4902

References

1. Fujino Y and Siringoringo DM. Bridge monitoring in Japan: the needs and strategies. *Struct Infrastruct Eng* 2011; 7(7-8): 597–611. DOI: 10.1080/15732479.2010.498282

2. Spencer BF, Jo H, Mechitov KA, et al. Recent advances in wireless smart sensors for multi-scale monitoring and control of civil infrastructure. *J Civil Struct Health Monitor* 2016; 6(1): 17–41.

3. Cunha A, Caetano E, Magalhaes F and Moutinho C. Recent perspectives in dynamic testing and monitoring of bridges. *Struct Control Health Monitor*. 2013; 20(6): 853–877. DOI: 10.1002/stc.1516

4. Figueiredo E and Brownjohn J. Three decades of statistical pattern recognition paradigm for SHM of bridges. *Struct Health Monitor* 2022: DOI: 10.1177/14759217221075241.

5. Guo T, Liu J, Zhang Y and Pan S. Displacement monitoring and analysis of expansion joints of long-span steel bridges with viscous dampers. *J Bridge Eng* 2015; 20(9): 04014099. DOI: 10.1061/(asce)be.1943-5592.0000701

6. Ni YQ, Hua XG, Wong KY and Ko JM. Assessment of bridge expansion joints using long-term displacement and temperature measurement. *J Perform Construct Facilit* 2007; 21(2): 143–151. DOI: 10.1061/(asce)0887-3828(2007)21:2(143)

7. Sun Z and Zhang Y. Failure mechanism of expansion joints in a suspension bridge. *J Bridge Eng* 2016; 21(10): 05016005. DOI: 10.1061/(asce)be.1943-5592.0000942

8. Li S, Niu J and Li Z. Novelty detection of cable-stayed bridges based on cable force correlation exploration using spatiotemporal graph convolutional networks. *Struct Health Monitor* 2021; 20(4): 2216–2228. DOI: 10.1177/1475921720988666

9. Li SL, Wei SY, Bao YQ and Li H. Condition assessment of cables by pattern recognition of vehicle-induced cable tension ratio. *Eng Struct* 2018; 155: 1–15. DOI: 10.1016/j.engstruct.2017.09.063

10. Sun Z, Ning S and Shen Y. Failure investigation and replacement implementation of short suspenders in a suspension bridge. *J Bridge Eng* 2017; 22(8): 05017007. DOI: 10.1061/(asce)be.1943-5592.0001089

11. Sun Z and Sun H. Jiangyin Bridge: An example of integrating structural health monitoring with bridge maintenance. *Struct Eng Int* 2018; 28(3): 353–356. DOI: 10.1080/10168664.2018.1462671

12. Wang F, Ning S and Sun Z. Experimental investigation on wear resistance of bushing in bridge suspenders. *J Performance Construct Facilit* 2020; 34(3): 06020001. DOI: 10.1061/(asce)cf.1943-5509.0001429

13. Lei XM, Sun LM and Xia Y. Lost data reconstruction for structural health monitoring using deep convolutional generative adversarial networks. *Struct Health Monitor* 2021; 20(4): 2069–2087. DOI: 10.1177/1475921720959226

14. Xia Y, Lei XM, Wang P, Liu GM and Sun LM. Long-term performance monitoring and assessment of concrete beam bridges using neutral axis indicator. *Struct Control Health Monitor* 2020; 27(12): e2637. DOI: 10.1002/stc.2637

15. Teng J, Tang D-H, Hu W-H, et al. Mechanism of the effect of temperature on frequency based on long-term monitoring of an arch bridge. *Struct Health Monitor* 2021; 20(4): 1716–1737. DOI: 10.1177/1475921720931370

16. Zhou Y, Xia Y, Sun Z and Fujino Y. Analytical formulation of the temperature-induced deformation of multi-span suspension bridges. *Struct Control Health Monitor* 2022; 29(6): e2937. DOI: 10.1002/stc.2937

17. Dan D, Yu X, Han F and Xu B. Research on dynamic behavior and traffic management decision-making of suspension bridge after vortex-induced vibration event. *Struct Health Monitor* 2021; 21(3): 14759217211011582. DOI: 10.1177/14759217211011582

18. Sun Z, Zou Z, Ying X and Li X. Tuned mass dampers for wind-induced vibration control of Chongqi bridge. *J Bridge Eng* 2020; 25(1): 05019013. DOI: 10.1061/(asce)be.1943-5592.0001510

19. Sun Z, Siringoringo DM and Fujino Y. Load-carrying capacity evaluation of girder bridge using moving vehicle. *Eng Struct* 2021; 229: 111645. DOI: 10.1016/j.engstruct.2020.111645

20. Sun Z and Zou Z. Towards an efficient method of predicting vehicle-induced response of bridge. *Eng Comput* 2016; 33(7): 2067–2089. DOI: 10.1108/ec-02-2015-0034

21. Cahill P, Hazra B, Karoumi R, Mathewson A and Pakrashi V. Vibration energy harvesting based monitoring of an operational bridge undergoing forced vibration and train passage. *Mech Syst Signal Process* 2018; 106: 265–283. DOI: 10.1016/j.ymssp.2018.01.007

22. Cantero D, Ülker-Kaustell M and Karoumi R. Time-frequency analysis of railway bridge response in forced vibration. *Mech Syst Signal Process* 2016; 76-77: 518–530. DOI: 10.1016/j.ymssp.2016.01.016

23. Mosleh A, Jara J, Razzaghi MS and Varum H. Probabilistic seismic performance analysis of RC bridges. *J Earthquake Eng* 2020; 24(11): 1704–1728. DOI: 10.1080/13632469.2018.1477637

24. Siringoringo DM and Fujino Y. Seismic response of a suspension bridge: Insights from long-term full-scale seismic monitoring system. *Struct Control Health Monitor* 2018; 25(11): e2252. DOI: 10.1002/stc.2252

25. Bayraktar A, Türker T, Tadla J, Kurşun A and Erdiş A. Static and dynamic field load testing of the long span Nissibi cable-stayed bridge. *Soil Dynam Earthquake Eng* 2017; 94: 136–157. DOI: 10.1016/j.soildyn.2017.01.019

26. Santos LO and Min X. Load tests of a cable-stayed bridge in Coimbra, Portugal. *Struct Eng Int* 2007; 17(4): 337–341.

27. Yinghong C, Yim J, Yang Z and Wang ML. Temperature effects on cable stayed bridge using health monitoring system: a case study. *Struct Health Monitor* 2010; 10(5): 523–537. DOI: 10.1177/1475921710388970

28. Zhou Y and Sun L. Insights into temperature effects on structural deformation of a cable-stayed bridge based on structural health monitoring. *Struct Health Monitor* 2019; 18(3): 778–791. DOI: 10.1177/1475921718773954

29. Liu C, Gong Y, Jiang Z and Guo K. Buffeting analysis of a suspension bridge under construction based on adjacent wind field data. *Eng Struct* 2022; 251: 113490. DOI: 10.1016/j.engstruct.2021.113490

30. Westgate R, Koo K-Y, Brownjohn J and List D. Suspension bridge response due to extreme vehicle loads. *Struct Infrastruct Eng* 2014; 10(6): 821–833. DOI: 10.1080/15732479.2013.767844

31. Brownjohn JMW, Koo K-Y, Scullion A and List D. Operational deformations in long-span bridges. *Struct Infrastruct Eng*. 2015; 11(4): 556–574. DOI: 10.1080/15732479.2014.951857

32. Jesus A, Brommer P, Westgate R, Koo K, Brownjohn J and Laory I. Bayesian structural identification of a long suspension bridge considering temperature and traffic load effects. *Struct Health Monitor* 2019; 18(4): 1310–1323. DOI: 10.1177/1475921718794299

33. Xia Y, Lei XM, Wang P and Sun LM. A data-driven approach for regional bridge condition assessment using inspection reports. *Struct Control Health Monitor* 2022; 29(4): e2915. DOI: 10.1002/stc.2915

34. Xia Y, Lei XM, Wang P and Sun LM. Artificial intelligence based structural assessment for regional short- and medium-span concrete beam bridges with inspection information. *Remote Sens* 2021; 13(18): 3687. DOI: 10.3390/rs13183687

35. Zhang Z and Sun C. Structural damage identification via physics-guided machine learning: a methodology integrating pattern recognition with finite element model updating. *Struct Health Monitor* 2021; 20(4): 1675–1688. DOI: 10.1177/1475921720927488

36. Fan G, Li J and Hao H. Dynamic response reconstruction for structural health monitoring using densely connected convolutional networks. *Struct Health Monitor* 2020; 20(4): 1373–1391. DOI: 10.1177/1475921720916881

37. Lei X, Xia Y, Dong Y and Sun L. Multi-level time-variant vulnerability assessment of deteriorating bridge networks with structural condition records. *Eng Struct* 2022; 266: 114581. DOI:10.1016/j.engstruct.2022.114581

38. Santos JP, Cremona C, Orcesi AD and Silveira P. Early damage detection based on pattern recognition and data fusion. *J Struct Eng* 2017; 143(2): 04016162. DOI:10.1061/(asce)st.1943-541x.0001643

39. Ni YQ, Hua XG, Fan KQ and Ko JM. Correlating modal properties with temperature using long-term monitoring data and support vector machine technique. *Eng Struct* 2005; 27(12): 1762–1773. DOI: 10.1016/j.engstruct.2005.02.020

40. Sun Z, Santos J and Caetano E. Vision and support vector machine–based train classification using weigh-in-motion data. *J Bridge Eng* 2022; 27(6): 06022001.

41. Zhang Z, Sun C and Guo B. Transfer-learning guided Bayesian model updating for damage identification considering modeling uncertainty. *Mech Syst Signal Process* 2022; 166: 166108426. DOI: 10.1016/j.ymssp.2021.108426

42. Bao Y and Li H. Machine learning paradigm for structural health monitoring. *Struct Health Monitor* 2021; 20(4): 1353–1372. DOI: 10.1177/1475921720972416

43. Hou R and Xia Y. Review on the new development of vibration-based damage identification for civil engineering structures: 2010-2019. *J Sound Vibrat* 2021; 491: 115741. DOI: 10.1016/j.jsv.2020.115741

44. Sun L, Shang Z, Xia Y, Bhowmick S and Nagarajaiah S. Review of bridge structural health monitoring aided by big data and artificial intelligence: from condition assessment to damage detection. *J Struct Eng* 2020; 146(5): 04020073. DOI: 10.1061/(asce)st.1943-541x.0002535

45. Ye XW, Jin T and Yun CB. A review on deep learning-based structural health monitoring of civil infrastructures. *Smart Struct Syst* 2019; 24(5): 567–585. DOI: 10.12989/sss.2019.24.5.567

46. Mao J, Wang H and Spencer BF. Toward data anomaly detection for automated structural health monitoring: exploiting generative adversarial nets and autoencoders. *Struct Health Monitor* 2020; 20(4): 1609–1626. DOI: 10.1177/1475921720924601

47. Song Q, Chen Y, Abdoli Oskoui E, et al. Micro-crack detection method of steel beam surface using stacked autoencoders on massive full-scale sensing strains. *Struct Health Monitor* 2020; 19(4): 1175–1187. DOI: 10.1177/1475921719879965

48. Wang Z and Cha Y-J. Unsupervised deep learning approach using a deep auto-encoder with an one-class support vector machine to detect structural damage. *Struct Health Monitor* 2020: 20(1): 406-425. DOI: 10.1177/1475921720934051.

49. Fernandez-Navamuel A, Magalhães F, Zamora-Sánchez D, Omella ÁJ, Garcia-Sanchez D and Pardo D. Deep learning enhanced principal component analysis for structural health monitoring. *Struct Health Monitor* 2022; 21(4): 1710–1722. DOI: 10.1177/14759217211041684

50. Sarwar MZ and Cantero D. Deep autoencoder architecture for bridge damage assessment using responses from several vehicles. *Eng Struct* 2021; 246: 113064. DOI: 10.1016/j.engstruct.2021.113064

51. Fan G, Li J and Hao H. Lost data recovery for structural health monitoring based on convolutional neural networks. *Struct Control Health Monitor* 2019; 26(10): e2433. DOI: 10.1002/stc.2433

52. Kang DH and Cha Y-J. Efficient attention-based deep encoder and decoder for automatic crack segmentation. *Struct Health Monitor* 2021; DOI: 10.1177/14759217211053776

53. Wang Z and Cha Y-J. Unsupervised deep learning approach using a deep auto-encoder with an one-class support vector machine to detect structural damage. *Struct Health Monitor* 2021; 20(1): 406–425. DOI: 10.1177/1475921720934051

54. Sun Z, Zou Z and Zhang Y. Utilization of structural health monitoring in long-span bridges: case studies. *Struct Control Health Monitor* 2017; 24(10): e1979. DOI: 10.1002/stc.1979

55. Zhou Y and Sun L. A comprehensive study of the thermal response of a long-span cable-stayed bridge: from monitoring phenomena to underlying mechanisms. *Mech Syst Signal Process* 2019; 124: 330–348. DOI: 10.1016/j.ymssp.2019.01.026

56. Cheadle C, Vawter MP, Freed WJ and Becker KG. Analysis of microarray data using Z score transformation. *J Mol Diagnost* 2003; 5(2): 73–81. DOI: 10.1016/s1525-1578(10)60455-2

57. Badrinarayanan V, Kendall A and Cipolla R. SegNet: a deep convolutional encoder-decoder architecture for image segmentation. *IEEE Trans Pattern Anal Mach Intell* 2017; 39(12): 2481–2495. DOI: 10.1109/tpami.2016.2644615

58. He KM, Zhang XY, Ren SQ and Sun J. Deep residual learning for image recognition. In: *2016 IEEE Conference on Computer Vision and Pattern Recognition*, 2016 pp.770–778. Las Vegas, NV: CVPR.

59. Hochreiter S and Schmidhuber J. Long short-term memory. *Neural Computat* 1997; 9(8): 1735–1780. DOI: 10.1162/neco.1997.9.8.1735

60. Yue Z, Ding Y, Zhao H and Wang Z. Mechanics-Guided optimization of an LSTM network for real-time modeling of temperature-induced deflection of a cable-stayed bridge. *Eng Struct* 2022; 252: 113619.